Magnetism in the Néel-skyrmion host GaV$_4$S$_8$ under pressure

T. J. Hicken [1,*] M. N. Wilson,[1] S. J. R. Holt [2] R. Khassanov,[3] M. R. Lees [2] R. Gupta,[3]
D. Das [3] G. Balakrishnan [2] and T. Lancaster [1]

[1]*Department of Physics, Centre for Materials Physics, Durham University, Durham DH1 3LE, United Kingdom*
[2]*Department of Physics, University of Warwick, Coventry CV4 7AL, United Kingdom*
[3]*Laboratory for Muon Spin Spectroscopy, Paul Scherrer Institute, 5232 Villigen PSI, Switzerland*

We present magnetization and muon-spin spectroscopy measurements of Néel-skyrmion host GaV$_4$S$_8$ under the application of hydrostatic pressures up to $P = 2.29$ GPa. Our results suggest that the magnetic phase diagram is altered with pressure via a reduction in the crossover temperature from the cycloidal (C) to ferromagnetic-like state with increasing P, such that, by 2.29 GPa, the C state appears to persist down to the lowest measured temperatures. With the aid of micromagnetic simulations, we propose that the driving mechanism behind this change is a reduction in the magnetic anisotropy of the system, and suggest that this could lead to an increase in stability of the skyrmion lattice.

I. INTRODUCTION

The lacunar spinel GaV$_4$S$_8$ [1] is one of very few examples of a material that hosts a magnetic Néel skyrmion lattice (SkL) [2] throughout the bulk [3]. The SkL, along with the cycloidal (C) phase, stabilized in different parts of the applied field-temperature (B-T) phase diagram, occurs due to a competition between magnetic exchange and the Dzyaloshinskii-Moriya interaction (DMI). The latter arises owing to the the polar rhombohedral structure ($R3m$) that GaV$_4$S$_8$ adopts below a structural phase transition at 42 K [4], generally attributed to a Jahn-Teller distortion. Above this temperature the material possesses a cubic $F\bar{4}3m$ structure. Also important in this material is easy-axis anisotropy [5], whose direction aligns with the rhombohedral distortion. Competition between the three interactions leads to a rich magnetic phase diagram, with dependence on the alignment between the applied magnetic field and crystallographic axes [3]. In zero field the ground state comprises a complex ferromagnetic-like (FM*) configuration, where the spins on the V atoms in each V$_4$ cluster combine to form effective spin-1/2 units that align ferromagnetically [6]. On increasing temperature, C ordering then takes place in the region $5 \lesssim T < T_c \simeq 13$ K. Under the application of an applied field, in polycrystalline samples of GaV$_4$S$_8$, the SkL phase is stabilized at $10 \lesssim T \lesssim 13$ K, $40 \lesssim \mu_0 H_{ext} \lesssim 100$ mT [7].

The application of hydrostatic pressure on GaV$_4$S$_8$ has been studied previously at room temperature [8]. Above 35 GPa there is a pressure-induced structural phase transition that results in the high-T cubic phase becoming orthorhombic ($Imm2$), alongside a semiconductor to metallic transition and changes in the optical properties of the material. At lower pressures, the changes in crystal structure are more modest, with a gradual reduction in the lattice parameter on increasing

pressure. Although there has been some effort to construct a magnetic T-P phase diagram of GaV$_4$S$_8$ [9], the transitions between the magnetically ordered states have not been thoroughly investigated.

We have previously studied the magnetism in the GaV$_4$S$_{8-y}$Se$_y$ series using magnetometry and muon-spin spectroscopy (μ^+SR) [7,10]. These techniques are sensitive to subtle changes in the magnetism of this series, revealing, for example, that the transition from FM* to C states is a crossover, rather than an abrupt phase transition [11,12]. This process is likely to depend sensitively on the crystalline anisotropy in the system [13], which has been shown to decrease as T increases [5]. Here we extend our investigation of GaV$_4$S$_8$ to probe the magnetic behavior under the application of hydrostatic pressure up to $P = 2.29$ GPa. With the aid of micromagnetic simulations, we interpret the effect of pressure in terms of changes to the relative strengths of terms appearing in an effective Hamiltonian.

II. EXPERIMENTAL AND COMPUTATIONAL DETAILS

Polycrystalline samples of GaV$_4$S$_8$ were synthesized and characterized as described in Refs. [10,14]. Measurements of the magnetization were made using a Quantum Design Magnetic Property Measurement System. The sample was loaded into a EasyLab Mcell pressure cell which allowed pressures of up to 1 GPa. The pressure was measured *in situ* by monitoring the superconducting transition of a tin manometer. Temperature scan measurements were performed in an applied magnetic field (either 10 mT or 5 T) on cooling from room temperature. Field scan measurements were performed on decreasing field at 2 K.

μ^+SR measurements [15–17] of polycrystalline GaV$_4$S$_8$ were carried out at the μE1 beamline of the Swiss Muon Source (SμS), Paul Scherrer Institute, Switzerland, using the GPD instrument. Both zero-field (ZF) measurements (where no external magnetic field is applied) and transverse-field (TF)

---

*Present address: Department of Physics, Royal Holloway, University of London, Egham TW20 0EX, United Kingdom.

measurements (where an external magnetic field is applied perpendicular to the initial muon-spin polarization) were performed. Polycrystalline samples were loaded in a double-wall piston cylinder cell made of MP35N material [18,19], using Daphne oil (7373) as a pressure-transmitting medium, which was mounted in a Janis cryostat. Data analysis was carried out using the WiMDA program [20] and made use of the MINUIT algorithm [21] via the iminuit [22] Python interface for global refinement of parameters. We have used the muon stopping sites calculated in Ref. [10], along with the MuESR code [23], to perform simulations of magnetic field distributions as seen with μ^+SR in GaV$_4$S$_8$.

Micromagnetic simulations were carried out using the ubermag package [24,25]. A $512 \times 512 \times 1$ grid of cells (side length 0.8 nm) with periodic boundary conditions in all directions was simulated. The C_{nv} crystal class was used, with micromagnetic parameters based on previous experimental and computational work [3,5,26]. We set exchange $\mathcal{A} = 0.05975$ pJ/m, DMI $D_0 = 0.03057$ mJ/m^2, magnetocrystalline anisotropy $K_0 = 16$ kJ/m^3, and saturation magnetization $M_s = 33.07$ kA/m. The easy axis $\boldsymbol{u}$ was out of the plane of the simulation, aligned with the magnetic field direction.

III. RESULTS AND DISCUSSION

The results of magnetization measurements made at several applied pressures are shown in Fig. 1. We start by considering the measurements performed under the application of a small $\mu_0 H = 10$ mT external field [Fig. 1(a)] with the intention of studying the system close to the magnetic ground state. In these measurements, the pressure cell adds a significant background to the measured magnetization. The data in Fig. 1(a) are therefore normalized to the maximum magnetization M_{max} at each pressure. There is no significant change in this quantity with pressure, which appears to vary randomly by a few percent. As the temperature is decreased, the measurements share the same features: (i) a small peak at $T \simeq 13$ K, (ii) a range of T where $M/M_{max} \lesssim 0.2$, and (iii) a rapid increase in the magnetization at low T.

We attribute each of the three features to different physical origins. (i) The peak at $T \simeq 13$ K marks T_c, which increases very slightly with pressure, although this change is small compared to other features. As T_c is set, predominantly, by the strength of the exchange interaction $\mathcal{A}$, we infer that pressure does not significantly change this parameter. (ii) The range of T where M/M_{max} is small corresponds to the C state, where the rotating spin structure leads to almost zero magnetization. (iii) The increase in magnetization as T decreases further is consistent with the crossover to the FM* phase. The sample magnetization does not increase further once the FM* state is stabilized over the entire sample. Pressure has a marked effect on the temperature at which the magnetization increase occurs, suggesting that as the pressure is increased, the C to FM* crossover occurs at successively lower T. There are two changes to the spin Hamiltonian that might explain this behavior: an increase in the strength of the DMI (making the twisting C state more preferable compared to the FM* state), or a decrease in the easy-axis anisotropy (making the spins
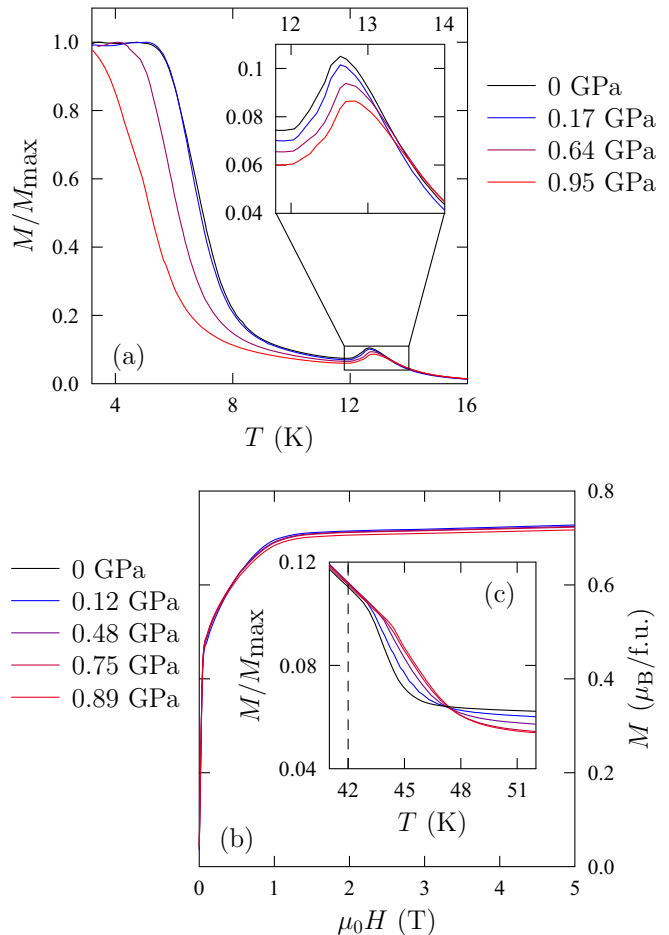

FIG. 1. Magnetization measurements of GaV$_4$S$_8$ under the application of various external pressures. (a) A temperature scan in an applied field of 10 mT. Data are normalized to the maximum magnetization at each pressure. Inset shows an enlargement of the region around $T_c \simeq 13$ K. (b) A field scan at 2 K. (c) The change in magnetization associated with the Jahn-Teller induced structural phase transition, measured in an applied field of 5 T. The 0 GPa measurements are performed without the pressure cell. As in (a), the data are normalized. The dashed line marks T_{JT} at $P = 0$ GPa according to Ref. [4].

less likely to align along a particular direction). These two possibilities are discussed in more detail below.

Measurements were also performed at $T = 2$ K as a function of applied field [Fig. 1(b)]. These results are not normalized, and show the magnetization saturates at effectively the same value regardless of applied pressure. There is a slight reduction in magnetization with increasing pressure; however this is very small ($<1.7\%$/GPa) and is therefore hard to unambiguously say whether this is an artifact from the pressure cell. The pressure cell does have a significant impact on the magnetization, hence the absolute values extracted should be treated with caution; the measured magnetization is significantly suppressed compared to measurements of the same samples measured outside of the pressure cell (where saturation is about 0.85 μ_B/f.u.).

Figure 1(c) shows the temperature dependence of the magnetization under the application of a $\mu_0 H = 5$ T external field,

where the system is in a field-polarized state below T_c, around the temperature below which the Jahn-Teller distortion occurs, T_{JT} (= 42 K at $P = 0$ [4]). As in Fig. 1(a), the data have been normalized. The effect of the pressure cell (proportionally larger above T_c due to the small sample signal) results in a pressure-independent shift of features to a slightly higher T. There appears to be a systematic increase in T_{JT} as P increases (around 1.3 K/GPa at these pressures). Reference [8] reports that above 35 GPa, at room temperature, the system adopts the $Imm2$ structure.

To further understand the crystal structures, and the effect of pressure, we can consider related chemically substituted systems, where the effect of substitution is similar to that of an external pressure. In $GaMo_4Se_8$, when the Jahn-Teller distortion is decomposed into different normal modes, it has been shown that [27] different amplitudes of these modes results in either the $F\bar{4}3m$ phase (stabilized in GaV_4S_8 at low P, low T), or $Imm2$ phase (stabilized in GaV_4S_8 at high P, high T). Further, Ref. [28] reports that $GaMo_4Se_8$ exhibits coexistence of the ground state $F\bar{4}3m$ structure and the metastable $Imm2$ structure at low T. In contrast, in GeV_4S_8, the structure below T_{JT} is $Imm2$ [29,30].

One possible explanation for the changes in the structure of GaV_4S_8 with pressure is that the transition observed at room temperature, $P \simeq 35$ GPa, is not the same as that observed at T_{JT} in the absence of applied pressure. An alternative, perhaps simpler, explanation could be that (i) T_{JT} increases with pressure in GaV_4S_8 such that T_{JT} is above room temperature for pressures above 35 GPa, and that (ii) changes to the nature of the distortion results in the realization of the $Imm2$ phase. For this scenario there would either need to be an increase in the rate of change of T_{JT} with pressure (extrapolating the rate from our data is not sufficient), or a discontinuous change in T_{JT} due to some significant change in the behavior of the system (which could be related to the realization of the $Imm2$ phase).

To further probe the magnetic phase diagram of GaV_4S_8, we performed μ^+SR measurements with the application of a weak transverse field (wTF), and in zero applied magnetic field (ZF). Previous μ^+SR measurements in this regime [7,10] revealed a complicated state of affairs with two classes of muon sites sensitive to both static and dynamic effects, with behavior likely resulting from the evolution of the magnetic structure and the magnetic domains with temperature. We first consider the wTF measurements, useful in determining the nature of magnetic transitions, which were performed in 3 mT applied perpendicular to the initial muon-spin direction. The measured asymmetry spectra $A_{wTF}(t)$ (example spectra are shown in the inset of Fig. 2(a), and in the Supplemental Material [17]) have two clear contributions from the precession of the muon spin, one from the response of muons predominantly sensitive to the external wTF (i.e., stopped outside the sample, or in positions where the internal field is small), and the other from muons that stop in sites dominated by the internal field in the material. The contribution from these second class of muon sites track the results we obtain with ZF μ^+SR discussed later, but with an expected larger uncertainty than the ZF measurement. We parametrize the data with

$$A_{wTF}(t) = a_r \cos(\gamma_\mu B_{wTF}) \exp(-\Lambda_r t) + a_b, \qquad (1)$$
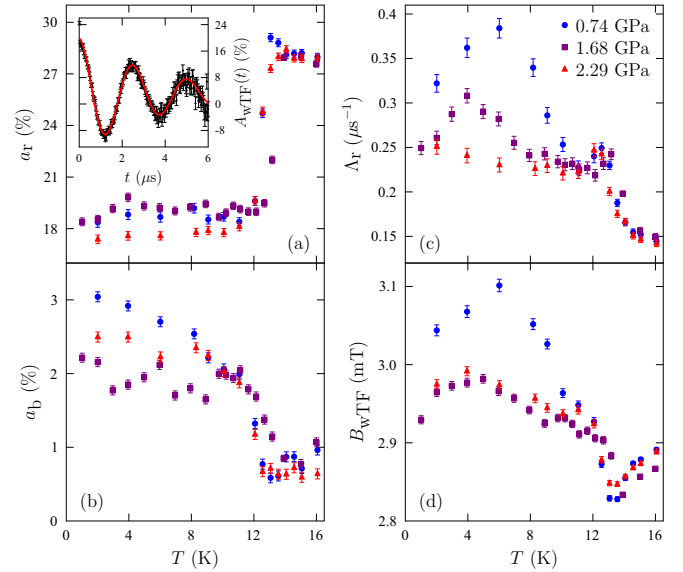

FIG. 2. Parameters extracted through fitting wTF μ^+SR measurements of GaV_4S_8 under various indicated external pressures in a applied field of 3 mT. Asymmetries are shown on the left [(a), (b)], with Λ_r and B_{wTF} on the right [(c), (d)] describing the effects of residual fields on muons outside the sample, or in positions of near cancellation of the internal field. The inset of (a) shows representative data measured at 2.29 GPa, 0.4 K, with the corresponding fit.

for all T, excluding the first 0.2 μs of data from the fits (where the spectra is dominated by the rapid precession and relaxation from muons stopping in the sites sensitive to the internal field). This approach captures contributions from all muon sites for $T > T_c$, but the oscillating component loses the contribution from those muon sites experiencing the large, internal magnetic field resulting from magnetic order below T_c. The results from this parametrization can be seen in Fig. 2.

The relaxing asymmetry a_r corresponds to muons stopping at sites where the field is B_{wTF}. The associated relaxation rate Λ_r can arise due to both static disorder (leading to a distribution of local magnetic fields at the muon sites, whose width determines the relaxation rate) and dynamic fluctuations on the muon timescale (where the amplitude and rate of the fluctuating field determines the relaxation rate). Note that the observed exponential relaxation usually corresponds to dynamic fluctuations. We find that a_r decreases below T_c as expected for a magnetic transition [Fig. 2(a)], where we usually see the loss of the signal from the magnetically ordered component of the sample. In this regime the temperature-dependent a_b [Fig. 2(b)] mainly captures the contribution from muons with their spins directed along the large, static internal field in the ordered regime (and hence do not precess). The temperature evolution of this component is slightly unusual, but likely reflects dynamic fluctuations that freeze out as $T \to 0$, leading to a recovery of a_b. The effect of pressure does not change a_r within the statistical accuracy of the data and we see no evidence for a pressure-induced magnetic phase separation from these results. Despite the gradual temperature evolution of a_b, these results, taken with the previous μ^+SR, suggest the entire sample shows long-range magnetic order below T_c at all pressures.
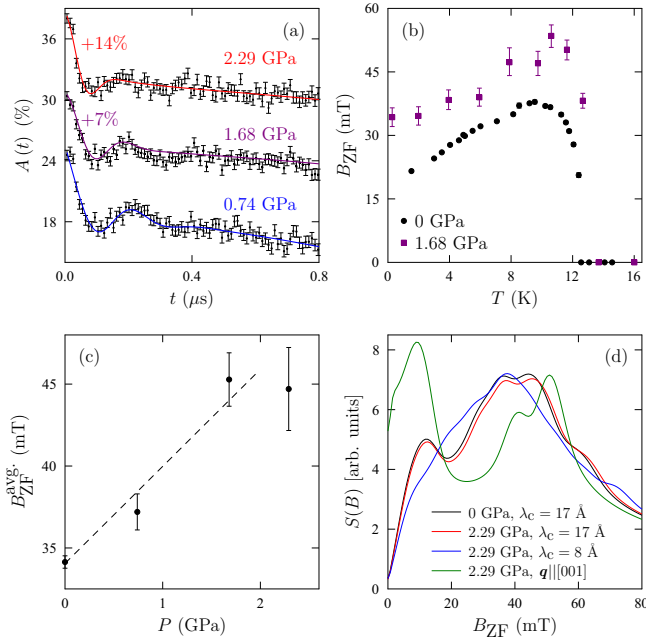
FIG. 3. (a) Example ZF μ^+SR asymmetry spectra of GaV$_4$S$_8$ at various pressures, all at 2 K. The internal field extracted from fitting the 1.68 GPa data is shown in (b), and compared to the zero-pressure result reported in Ref. [7]. All other measured pressures show the same shape [17]. The average internal field for 8 K $< T < T_c$ (i.e., in the C phase at all pressures) at each pressure is shown in (c). (d) Simulations of the internal field distribution as seen with ZF μ^+SR for the cycloidal state in GaV$_4$S$_8$ under various different possible conditions.

We now consider Λ_r and B_{wTF} [Figs. 2(c)–2(d)], whose behavior below T_c reflects muons stopping outside the sample or in positions where the internal field is small. Considering first the low-temperature FM* to C transition, at 0.74 GPa, both Λ_r and B_{wTF} show a local maximum coincident with the crossover, consistent with magnetometry results and a similar peak in the relaxation rate observed at ambient pressure [7]. As P is increased, these peaks are pushed to lower T (consistent with the magnetization results), before the peak becomes impossible to resolve at 2.29 GPa, suggesting the C state persists down to lower T than measured. A peak in Λ_r is not unexpected for a phase transition or crossover; however, the peak in B_{wTF} is more unusual. We suggest that since, as T increases, the anisotropy in GaV$_4$S$_8$ decreases [5], this will lead to a changing orientational preference of the magnetic domains in the sample, altering the magnetic field experienced by the muons outside the sample due to the macroscopic fields from the different grains. The field experienced by the muons will then peak in the FM* state when domains are most aligned, which should occur at the highest temperature where the FM* state is realized. The peak in B_{wTF}, therefore, coincides with the transition between the FM* and C states.

ZF μ^+SR measurements were also performed as a function of pressure, with example spectra shown in Fig. 3(a). Below T_c the asymmetry spectra $A(t)$ are well described by

$$A(t) = a_1 \cos\left(\gamma_\mu B_{ZF} + \phi\right) \exp\left(-\sigma_1^2 t^2\right)$$
$$+ a_2 \exp\left(-\Lambda_2 t\right) + a_3 \exp\left(-\sigma_3^2 t^2\right) + a_4. \quad (2)$$

Above T_c only the a_3 and a_4 terms are needed. The first term in Eq. (2) accounts for contributions from muon-spin components initially perpendicular to the local field B_{ZF}, leading to coherent spin precession, whereas the second term accounts for components initially parallel to the local field, which relax due to dynamics in the local field distribution. In these measurements, there is a significant contribution from the pressure cell, which is captured by the third and fourth terms, leading to several parameters that are temperature independent: $a_1/(a_1 + a_2 + a_3)$, $a_2/(a_1 + a_2 + a_3)$, $a_3/(a_1 + a_2 + a_3)$. We find that $a_1 + a_2 + a_3$ increases with T, and σ_3, and a_4 predominantly capture the temperature dependence of the cell. We are unable to extract any useful information from Λ_2 (which is determined by dynamic fluctuations). We also find that σ_1 (likely to be determined by a mixture of static disorder and residual dynamics) is temperature independent, and hence was refined simultaneously at all T. The most interesting parameter is therefore the internal field B_{ZF} [Fig. 3(b)]. (The behavior we observe here contrasts with our previous work [7] where two internal fields were detected, one higher field, broadly matching the low-pressure B_{ZF} found here, and one lower field, which is not observable in this configuration, likely due to the competing signal from the pressure cell.) At all pressures, B_{ZF} increases slightly with increasing T, as previously observed [7] (shown for comparison), before collapsing to zero above T_c as expected.

Despite no notable changes in the saturation magnetization with pressure [Fig. 1(b)], the local internal field significantly increases as the pressure is increased, as shown in Fig. 3(c). This suggests a change to the structure of the C state that does not lead to a change in the net magnetization of the FM* state. To explore possibilities that explain this, we consider the changes to the Hamiltonian previously suggested: an increase in the DMI, or a decrease in the anisotropy. An increase in DMI with pressure would be expected to lead to a decrease in the cycloidal period (as the wavelength $\lambda_C \propto \mathcal{A}/D$). We can simulate the effect this change in the period would have on the distribution of fields seen at the muon site following the approach in Ref. [7], which was shown to describe the ZF μ^+SR data. The values of σ_1 and Λ_2 are the same order of magnitude as the comparable parameters Λ_i in Ref. [7], suggesting the width of the distribution of magnetic fields at the muon site remains similar upon application of pressure. We therefore conclude that the simulations are likely still good descriptors of the ZF μ^+SR data.

The simulated distribution [7] produced for the experimentally observed C state ($\lambda_C = 17$ nm, and the *q*-vector perpendicular to the [001] direction [31]) is shown in Fig. 3(d). We first consider the effect on the distribution that the small change in lattice parameters arising due to the pressure would have. Taking the change in cell volume from Ref. [8], and assuming the muon sites remain unchanged (a reasonable assumption given the minimal change to the lattice parameters), we can see that the spectrum is almost unchanged. Reducing the cycloidal period to $\lambda_C = 8$ nm (equivalent to approximately doubling the relative strength of the DMI) changes the form, but not the position of the features (i.e., B_{ZF}) in the spectrum. It is therefore unlikely that this can explain the observed increase in internal field. Further, as changes to $\mathcal{A}$ would also result in changes to λ_C, these results
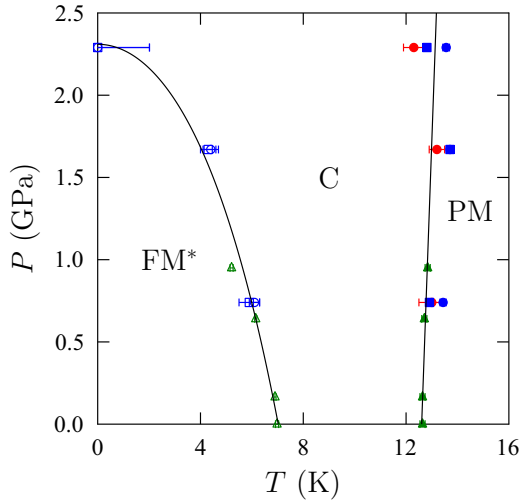
FIG. 4. *P-T* dependence of GaV$_4$S$_8$ based on magnetization (green) and μ^+SR (ZF: red; wTF: blue) measurements. Closed symbols indicate T_c, above which the system is paramagnetic (PM), and open symbols represent the ferromagnetic-like (FM*) to cycloidal (C) transition. Circles indicate the point that comes from the extracted value of the internal field [Fig. 2(d), Fig. 3(b)], squares represent points from a feature in Λ_r [Fig. 2(c)], and triangles represent points from magnetization [Fig. 1(a)]. The points are extracted as detailed in Table I.

TABLE I. Method of extracting transition temperatures shown in Fig. 4 from different measurement types.

Measurement	Parameter	Transition	Extracted feature
Magnetization	M	T_c	Local maximum
	M	FM* → C	$M = M_{max}/2$
wTF μ^+SR	Λ_r	T_c	Local maximum
	Λ_r	FM* → C	Local maximum
	B_{wTF}	T_c	Local minimum
	B_{wTF}	FM* → C	Local maximum
ZF μ^+SR	B_{ZF}	T_c	$B_{ZF} = 0$

also support the conclusion from the magnetization measurements that $\mathcal{A}$ does not significantly change with pressure.

One possible effect of a reduction in the anisotropy as the pressure is increased could be a changed preference for the direction of the $\boldsymbol{q}$-vector of the cycloidal state. In Fig. 3(d) we show that, if the $\boldsymbol{q}$-vector were to point along the [001] direction, the larger-field peak is shifted to higher fields, as seen experimentally. We note that changing the $\boldsymbol{q}$-vector was the only way we could find to simulate the observed increase in internal field without changing the net magnetization. While we cannot say for certain that this is the only orientation of the $\boldsymbol{q}$-vector that would reproduce this result, we found no other feasible direction when randomly sampling, or testing specific high symmetry directions. We, therefore, suggest that a change in the anisotropy is a possible explanation for both the reduction in temperature of the C to FM* crossover, and the increase in internal field with increasing pressure.

We have summarized our magnetization and μ^+SR results with a suggested *P-T* phase diagram in the absence of an applied field, Fig. 4. We have extracted the transition temperatures from the different types of measurement as shown in Table I. We find that T_c slightly increases with applied pressure, whereas the C to FM* crossover decreases in T as the pressure increases. The error bar on the highest-pressure, low-temperature point represents the minimum temperature we were able to measure.

To further study the effects on the magnetic states of these possible changes in the DMI and/or anisotropy, we have performed micromagnetic simulations. We use the Hamiltonian

$$\hat{\mathcal{H}} = -\mathcal{A}\boldsymbol{m} \cdot \nabla^2 \boldsymbol{m} + D(\boldsymbol{m} \cdot \nabla m_z - m_z \nabla \cdot \boldsymbol{m})$$
$$- K(\boldsymbol{m} \cdot \boldsymbol{u})^2 - \mu_0 M_s \boldsymbol{m} \cdot \boldsymbol{H}, \qquad (3)$$

which is appropriate for a C_{nv} crystal system, with the micromagnetic parameters defined in Sec. II. The exchange $\mathcal{A}$ term attempts to locally align $\boldsymbol{m}$ whereas the DMI D term prefers periodic rotation of $\boldsymbol{m}$. The anisotropy K term gives a preference for alignment along the easy axis $\boldsymbol{u}$, and the final term lowers the energy when $\boldsymbol{m}$ is aligned along the external field $\boldsymbol{H}$. We initialize different magnetic configurations before allowing the micromagnetic solver to find a local energy minimum, allowing us to probe the energy of many possible states.

In the absence of an applied field we find that the FM state is the most energetically favorable, with the C state only slightly higher in energy. (Note that, on the length scale of this simulation, each micromagnetic cell contains around four V$_4$ clusters, hence the FM* and FM state are indistinguishable.) An example of the C state simulated can be seen in Fig. 5(a). We study the effect of changing the D and K parameters, keeping the other parameters fixed, and identify the difference in energy between the lowest-energy C state (i.e., that which has the preferred C period) and the FM state. This is shown in Fig. 5(b), where the lowest-energy state is marked. As expected, both increasing D and decreasing K change the preferred state from FM to C. The minimum-energy cycloidal period is shown in Fig. 5(c), and shows that changes in λ_C are mainly correlated with changes in D.

Having established micromagnetics can reproduce the observed states, we can examine the effect of applying a magnetic field. We consider the energy of the skyrmion lattice (SkL) state compared to the ground state (either FM or C, depending on the micromagnetic parameters chosen). We find that, for D_0, K_0 (i.e., the zero-temperature parameters we expect in the absence of any applied pressure), the SkL state is hard to stabilize, with very few initialized SkL states retaining this character. The SkL state is never found to be lower in energy than the C or FM state, as expected from the measured phase diagram, where the SkL is only stabilized via thermal fluctuations above $T = 0$ in an applied field, typically over a range of 2–3 K below T_c. Changing the values of D and K makes stabilizing the SkL much more probable, with many more initialized SkL states staying in that configuration, and the energy of the skyrmion state above the ground state (normally C, apart from at high field in the $D = D_0$, $K = 0$ case where the ground state becomes FM) is much reduced. These micromagnetic simulations therefore suggest that, if the effect of changing pressure is a change in the D or K parameters, the SkL should still be stabilized at elevated temperatures, as
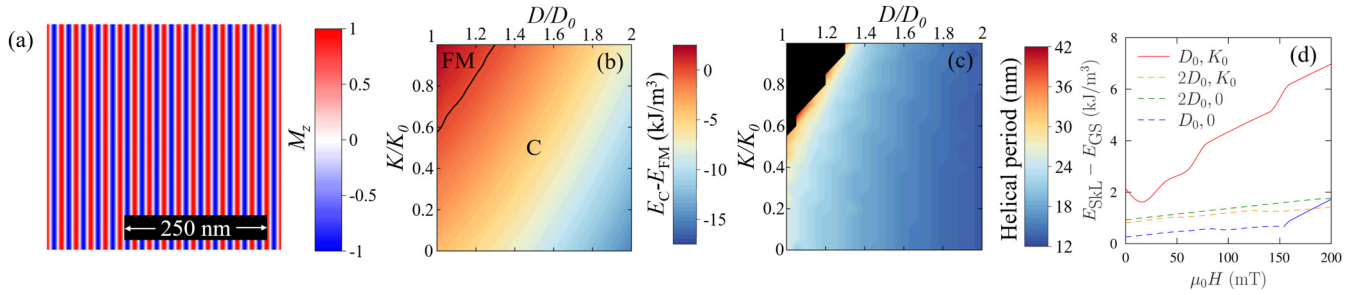
FIG. 5. Results of micromagnetic simulations using the parameters in Sec. II. (a) An example cycloidal (C) state. (b) Difference in energies between the C and ferromagnetic (FM) states as a function of D and K, with the preferred cycloidal period shown in (c). (d) Energies of the skyrmion lattice (SkL) state compared to the ground state (either FM, solid line, or C, dashed line) as a function of applied magnetic field for different combinations of D and K.

it is in the absence of an applied pressure, but with it likely to persist down to lower T. However, since the SkL is still never found to be the lowest-energy state it is unlikely to ever be stabilized at zero temperature.

TF μ^+SR has previously been shown to be able to identify the SkL phase in GaV$_4$S$_8$ via an increase in the internal field and the associated relaxation rate [7]. We have performed TF μ^+SR measurements of GaV$_4$S$_8$ at 50 mT and 100 mT (fields which stabilize a SkL in the absence of applied pressure) under the application of pressure. The asymmetry spectra $A_{\text{TF}}(t)$ are well described by

$$A_{\text{TF}}(t) = \sum_{i=1}^{2} a_i \cos\left(\gamma_\mu B_{\text{TF},i} + \phi_i\right) \exp\left(-\sigma_i^2 t^2\right) + a_{\text{b}}. \quad (4)$$

The $i = 2$ term captures the effects of muons stopping in the pressure cell when the spins subsequently precess; hence we employed simultaneous refinement of the associated temperature-independent parameters: $B_{\text{TF},2}$, ϕ_2, and σ_2. The total asymmetry $a_1 + a_2$ increases at T_c as expected, with a_{b} capturing temperature dependence that appears to be coming from the cell. The first term, sensitive to the magnetism in GaV$_4$S$_8$, has a temperature-independent ϕ_1 which was simultaneously refined at all temperatures. The remaining parameters $B_{\text{TF},1}$ and σ_1 are shown in Fig. 6.

At all applied pressures, the behavior is broadly similar in both parameters. We first consider the measured internal field, Figs. 6(a) and 6(c). At 50 mT, there is an enhancement of B_{TF} compared to the applied field, as previously seen in the absence of applied pressure [7]. There is no large increase in this parameter over a limited temperature range that would signify the stabilization of the SkL in that region, as has previously been observed at ambient pressure. Instead, the internal field seems enhanced for all $T < T_c$. Comparatively, at 100 mT the enhancement from the applied field is smaller.

Considering now the relaxation rate σ [Figs. 6(b) and 6(d)], we resolve two clear regimes of behavior at 0.81 GPa and 1.68 GPa in both the 50 mT and 100 mT measurements, as marked by dashed lines. The crossover T between these two regimes decreases as the pressure is increased, following a similar trend seen earlier for the FM* to C transition. By 2.23 GPa it is difficult to split the behavior into separate regimes, again as seen in the zero-field data. We conclude, therefore, that pressure acts to reduce the characteristic temperature scales of the magnetic field fluctuations in this part

of the phase diagram. We stress that we are unable to resolve those features seen at ambient pressure [7] that unambiguously mark the onset of the SkL. However, since fluctuations in the field distribution experienced by the muon have previously been shown to track the onset of the skyrmion phase, we might speculate that these data are consistent with the SkL phase extending to lower T, as anticipated from the micromagnetic results. The phase diagram would therefore look more like that of GaV$_4$Se$_8$, which has a SkL stable down to low T [32].

IV. CONCLUSION

Our magnetization and μ^+SR measurements of GaV$_4$S$_8$ reveal that the application of pressure lowers the crossover temperature of the C to FM* transition. By 2.29 GPa, we cannot observe this crossover, and suggest that GaV$_4$S$_8$ remains in the C state down to the lowest measured temperatures. On increasing the applied pressure, the internal field as measured by μ^+SR increases without any corresponding increase in the magnetization. Through simulations of the distribution of
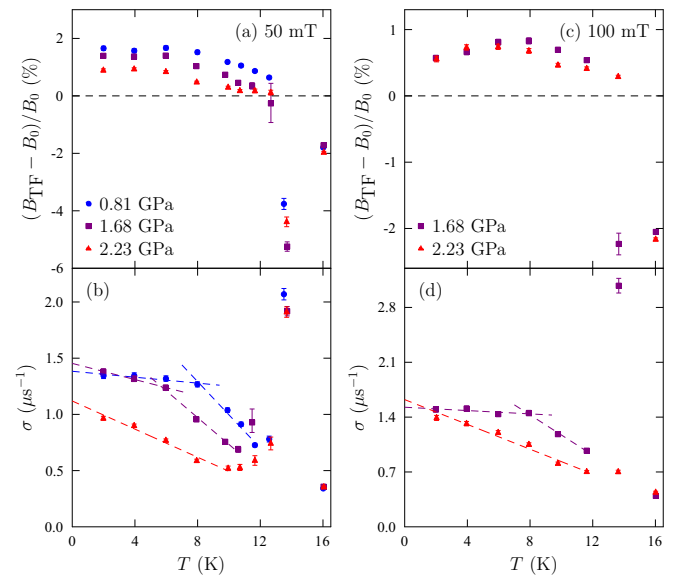

FIG. 6. Measured field shift [(a), (c)] and associated relaxation rate [(b), (d)] extracted from fitting of TF μ^+SR measurements of GaV$_4$S$_8$ at different applied pressures and magnetic fields B_0. Dashed lines in (b) and (d) are guides to the eye.

magnetic fields at the muon stopping sites, we suggest this occurs due to a reorientation of the direction of the q-vectors due to a reduction in the magnetic anisotropy of the system. Investigation of this phenomena with a q-resolved experimental probe would be highly beneficial in a future study. Micromagnetic simulations suggest further that a decrease in the magnetic anisotropy should lead to an increase in stability of the SkL state in GaV_4S_8.

There are multiple reasons that application of pressure may change the anisotropy of the system. The effect of pressure might be to make the underlying electronic structure more isotropic, hence explaining the above results. Further, the appearance of an easy axis in the system is set by the direction of the Jahn-Teller distortion; given our results on the increase of the temperature of the Jahn-Teller distortion with pressure, and the possibility of the changing nature of this distortion, it seems highly likely that the anisotropy would also have corresponding changes with pressure. Given the possible different scenarios we set out to explain the changes to the Jahn-Teller distortion with pressure, experiments to determine the crystal structure of GaV_4S_8 as a function of both temperature and pressure are an area of research that should be explored.

Our work shows the sensitivity of the magnetism in GaV_4S_8 to applied pressures, and demonstrates that changes in both the magnetic phase diagram and underlying magnetic interaction strengths can be expected. This provides the opportunity to tailor the magnetic interactions of this system, and perhaps related systems in the $GaV_4S_{8-y}Se_y$ series, and investigate the effects on the magnetism. Understanding the changes these parameters make is of great importance for understanding the behavior of these complex magnetic states, which is essential if they are to be used for applications.

Research data from this paper are available [33].

[1] D. Brasen, J. M. Vandenberg, M. Robbins, R. H. Willens, W. A. Reed, R. C. Sherwood, and X. J. Pinder, Magnetic and crystallographic properties of spinels of the type $A_xB_2S_4$ where $A =$ Al, Ga, and $B =$ Mo, V, Cr, J. Solid State Chem. **13**, 298 (1975).

[2] T. Lancaster, Skyrmions in magnetic materials, Contemp. Phys. **60**, 246 (2019).

[3] I. Kézsmárki, S. Bordács, P. Milde, E. Neuber, L. M. Eng, J. S. White, H. M. Rønnow, C. D. Dewhurst, M. Mochizuki, K. Yanai et al., Néel-type skyrmion lattice with confined orientation in the polar magnetic semiconductor GaV_4S_8, Nat. Mater. **14**, 1116 (2015).

[4] S. J. R. Holt, A. Štefančič, C. Ritter, A. E. Hall, M. R. Lees, and G. Balakrishnan, Structure and magnetism of the skyrmion hosting family $GaV_4S_{8-y}Se_y$ with low levels of substitutions between $0 \leqslant y \leqslant 0.5$ and $7.5 \leqslant y \leqslant 8$, Phys. Rev. Materials **4**, 114413 (2020).

[5] D. Ehlers, I. Stasinopoulos, I. Kézsmárki, T. Fehér, V. Tsurkan, H.-A. Krug von Nidda, D. Grundler, and A. Loidl, Exchange anisotropy in the skyrmion host GaV_4S_8, J. Phys.: Condens. Matter **29**, 065803 (2017).

[6] S. J. R. Holt, C. Ritter, M. R. Lees, and G. Balakrishnan, Investigation of the magnetic ground state of GaV_4S_8 using powder neutron diffraction, J. Phys.: Condens. Matter **33**, 255802 (2021).

[7] T. J. Hicken, S. J. R. Holt, K. J. A. Franke, Z. Hawkhead, A. Štefančič, M. N. Wilson, M. Gomilšek, B. M. Huddart, S. J. Clark, M. R. Lees et al., Magnetism and Néel skyrmion dynamics in $GaV_4S_{8-y}Se_y$, Phys. Rev. Research **2**, 032001(R) (2020).

[8] Y. Wang, S. Rahman, E. Sun, C. Knill, D. Zhang, L. Wang, V. Tsurkan, and I. Kézsmárki, From semiconducting to metallic: Jahn-Teller-induced phase transformation in skyrmion host GaV_4S_8, J. Phys. Chem. C **125**, 5771 (2021).

[9] J. Mokdad, G. Knebel, C. Marin, J.-P. Brison, V. Ta Phuoc, R. Sopracase, C. Colin, and D. Braithwaite, Structural, magnetic, and insulator-to-metal transitions under pressure in the GaV_4S_8 Mott insulator: A rich phase diagram up to 14.7 GPa, Phys. Rev. B **100**, 245101 (2019).

[10] K. J. A. Franke, B. M. Huddart, T. J. Hicken, F. Xiao, S. J. Blundell, F. L. Pratt, M. Crisanti, J. A. T. Barker, S. J. Clark, A. Štefančič et al., Magnetic phases of skyrmion-hosting $GaV_4S_{8-y}Se_y$ ($y = 0, 2, 4, 8$) probed with muon spectroscopy, Phys. Rev. B **98**, 054428 (2018).

[11] J. S. White, Á. Butykai, R. Cubitt, D. Honecker, C. D. Dewhurst, L. F. Kiss, V. Tsurkan, and S. Bordács, Direct evidence for cycloidal modulations in the thermal-fluctuation-stabilized spin spiral and skyrmion states of GaV_4S_8, Phys. Rev. B **97**, 020401(R) (2018).

[12] E. M. Clements, R. Das, G. Pokharel, M. H. Phan, A. D. Christianson, D. Mandrus, J. C. Prestigiacomo, M. S. Osofsky, and H. Srikanth, Robust cycloid crossover driven by anisotropy in the skyrmion host GaV_4S_8, Phys. Rev. B **101**, 094425 (2020).

[13] Y. A. Izyumov, Modulated, or long-periodic, magnetic structures of crystals, Sov. Phys. Usp. **27**, 845 (1984).

[14] A. Štefančič, S. J. Holt, M. R. Lees, C. Ritter, M. J. Gutmann, T. Lancaster, and G. Balakrishnan, Establishing magneto-structural relationships in the solid solutions of the skyrmion hosting family of materials: $GaV_4S_{8-y}Se_y$, Sci. Rep. **10**, 9813 (2020).

[15] S. J. Blundell, Spin-polarized muons in condensed matter physics, Contemp. Phys. **40**, 175 (1999).

[16] S. J. Blundell, R. De Renzi, T. Lancaster, and F. L. Pratt, *Muon Spectroscopy: An Introduction* (Oxford University Press, Oxford, 2021).

[17] See Supplemental Material at http://link.aps.org/supplemental/10.1103/PhysRevB.105.134414 for further information on the μ^+SR technique, and some additional data.

[18] R. Khasanov, Z. Guguchia, A. Maisuradze, D. Andreica, M. Elender, A. Raselli, Z. Shermadini, T. Goko, F. Knecht,

E. Morenzoni *et al.*, High pressure research using muons at the Paul Scherrer Institute, High Press. Res. **36**, 140 (2016).

[19] Z. Shermadini, R. Khasanov, M. Elender, G. Simutis, Z. Guguchia, K. V. Kamenev, and A. Amato, A low-background piston-cylinder-type hybrid high pressure cell for muon-spin rotation/relaxation experiments, High Press. Res. **37**, 449 (2017).

[20] F. L. Pratt, WiMDA: A muon data analysis program for the Windows PC, Phys. B: Condens. Matter **289-290**, 710 (2000).

[21] F. James and M. Roos, MINUIT: A system for function minimization and analysis of the parameter errors and corrections, Comput. Phys. Commun. **10**, 343 (1975).

[22] iminuit Team, iminuit: A Python interface to MINUIT, https://github.com/scikit-hep/iminuit.

[23] P. Bonfà, I. J. Onuorah, and R. De Renzi, Introduction and a quick look at MUESR, the magnetic structure and mUon embedding site refinement suite, JPS Conf. Proc. **21**, 011052 (2018).

[24] M. Beg, R. A. Pepper, and H. Fangohr, User interfaces for computational science: A domain specific language for OOMMF embedded in Python, AIP Adv. **7**, 056025 (2017).

[25] M. Beg, M. Lang, and H. Fangohr, Ubermag: Toward more effective micromagnetic workflows, IEEE Trans. Magn. **58**, 7300205 (2022).

[26] P. Padmanabhan, F. Sekiguchi, R. B. Versteeg, E. Slivina, V. Tsurkan, S. Bordács, I. Kézsmárki, and P. H. M. van Loosdrecht, Optically Driven Collective Spin Excitations and Magnetization Dynamics in the Néel-Type Skyrmion Host GaV_4S_8, Phys. Rev. Lett. **122**, 107203 (2019).

[27] K. Routledge, P. Vir, N. Cook, P. A. E. Murgatroyd, S. J. Ahmed, S. N. Savvin, J. B. Claridge, and J. Alaria, Mode crystallography analysis through the structural phase transition and magnetic critical behavior of the lacunar spinel $GaMo_4Se_8$, Chem. Mater. **33**, 5718 (2021).

[28] E. C. Schueller, D. A. Kitchaev, J. L. Zuo, J. D. Bocarsly, J. A. Cooley, A. Van der Ven, S. D. Wilson, and R. Seshadri, Structural evolution and skyrmionic phase diagram of the lacunar spinel $GaMo_4Se_8$, Phys. Rev. Materials **4**, 064402 (2020).

[29] H. Müller, W. Kockelmann, and D. Johrendt, The magnetic structure and electronic ground states of Mott insulators GeV_4S_8 and GaV_4S_8, Chem. Mater. **18**, 2174 (2006).

[30] D. Bichler, V. Zinth, D. Johrendt, O. Heyer, M. K. Forthaus, T. Lorenz, and M. M. Abd-Elmeguid, Structural and magnetic phase transitions of the V_4-cluster compound GeV_4S_8, Phys. Rev. B **77**, 212102 (2008).

[31] E. Ruff, S. Widmann, P. Lunkenheimer, V. Tsurkan, S. Bordács, I. Kézsmárki, and A. Loidl, Multiferroicity and skyrmions carrying electric polarization in GaV_4S_8, Sci. Adv. **1**, e1500916 (2015).

[32] Y. Fujima, N. Abe, Y. Tokunaga, and T. Arima, Thermodynamically stable skyrmion lattice at low temperatures in a bulk crystal of lacunar spinel GaV_4Se_8, Phys. Rev. B **95**, 180410(R) (2017).

[33] See http://doi.org/10.15128/r1dj52w474g.